

# SimuScene: Training and Benchmarking Code Generation to Simulate Physical Scenarios

Yanan Wang<sup>1,\*</sup>, Renxi Wang<sup>1,\*</sup>, Yongxin Wang<sup>1,\*</sup>, Xuezhi Liang<sup>1</sup>, Fajri Koto<sup>1</sup>, Timothy Baldwin<sup>1</sup>, Xiaodan Liang<sup>1,2,†</sup>, Haonan Li<sup>1,†</sup>

<sup>1</sup>Mohamed bin Zayed University of Artificial Intelligence (MBZUAI), Abu Dhabi, UAE

<sup>2</sup>Sun Yat-sen University (SYSU), Guangzhou, China

<https://yanan-wang-cs.github.io/SimuScene/>

## Abstract

Large language models (LLMs) have been extensively studied for tasks like math competitions, complex coding, and scientific reasoning, yet their ability to accurately represent and simulate physical scenarios via code remains underexplored. We propose SimuScene, the first systematic study that trains and evaluates LLMs on simulating physical scenarios across five physics domains and 52 physical concepts. We build an automatic pipeline to collect data, with human verification to ensure quality. The final dataset contains 7,659 physical scenarios with 334 human-verified examples as the test set. We evaluated 10 contemporary LLMs and found that even the strongest model achieves only a 21.5% pass rate, demonstrating the difficulty of the task. Finally, we introduce a reinforcement learning pipeline with visual rewards that uses a vision-language model as a judge to train textual models. Experiments show that training with our data improves physical simulation via code while substantially enhancing general code generation performance.

## 1. Introduction

Modern large language models (LLMs) (OpenAI, 2025b; DeepSeek-AI, 2025; Qwen, 2025; Cheng et al., 2025a) have impressive reasoning capabilities, as validated and measured over various tasks like math (MAA, 2024), coding (Liu et al., 2023; Jain et al., 2024), science (Xu et al., 2025a; Zhang et al., 2025a), and complex agent tasks (Luo et al., 2025; Merrill et al., 2026). While LLMs have achieved super-human performance on most benchmarks, we identify

a new type of task that hasn't been explored before: using code to simulate physical scenarios. Different from previous tasks, physical scenarios are inherently tied to motion and dynamic processes. Simulating this process requires a deep understanding of physical knowledge and a strong coding capability to represent physical objects accurately. These properties make it a suitable task for evaluating LLMs, combining awareness of the physical world and coding capabilities.

In this paper, we introduce **Physical Scenario Simulation (SimuScene)**, a novel task for evaluating the ability of LLMs to generate executable code simulations that are consistent with textual descriptions of physical scenarios. Rather than targeting numerically-accurate physical modeling, SimuScene focuses on the generation of simulations that respect basic physical constraints and match the qualitative motion described in language.

To construct the dataset, we propose an automatic pipeline: starting from 52 physical concepts across five domains, we use GPT-4o (OpenAI, 2024) to generate basic scenarios that are progressively enriched with additional conditions to control difficulty. Each scenario is validated for physical plausibility, paired with verification questions describing expected motion, and further refined using DeepSeek-R1-0528 (DeepSeek-AI, 2025) to cross-validate data quality (more details in § 3).

This pipeline yields the SimuScene dataset, comprising 7,659 dynamic scenarios across five major domains: mechanics, electromagnetism, optics, fluid mechanics, and thermodynamics. Each scenario centers on one core concept, with one to three additional conditions controlling difficulty. To support reliable evaluation, we curated a test set of 334 human-verified scenarios, where each scenario contains at least 4 verification questions. The remaining data are used for training; manual inspection of 100 randomly-sampled training examples shows an average quality rate of 84%, indicating the robustness of our automated data construction pipeline. Representative examples and their corresponding

<sup>\*</sup>Equal contribution . Correspondence to: Haonan Li <haonan.li@mbzuai.ac.ae>, Xiaodan Liang <xiaodan.liang@mbzuai.ac.ae>.

video simulations are shown in Fig. 1.

We evaluate 10 state-of-the-art LLMs on SimuScene and find that the best-performing model achieves only a 21.5% pass rate (average@8). These results indicate that existing LLMs struggle to generate executable simulations that are consistent with textual descriptions and exhibit plausible dynamic behavior, and demonstrate that SimuScene is a challenging benchmark for evaluating scene-level understanding and code generation capabilities.

Finally, we explore whether training can improve model performance on these simulation-oriented tasks. We introduce a vision-verifiable reward signal based on the generated simulation videos, together with several design choices that provide stable and fine-grained feedback in language-model-as-judge reinforcement learning, complemented by a detailed human evaluation. To our knowledge, this work is among the first to incorporate a vision-based reward signal for training text-only language models.

Using this reward setting, we train smaller models with SimuScene. Experimental results show that models trained under this setup achieve substantially better alignment between textual descriptions and simulated motions. Notably, our trained 7B model achieves an 11.1% pass rate, compared to 0% for the baseline model, demonstrating the effectiveness of our dataset and training method. Moreover, when mixing our data with a general instruction-following dataset (OpenThoughts (Guha et al., 2025)), we observe substantial improvements in coding performance without degradation on other benchmarks or domains.

To summarize, our contributions are three-fold:

1. We present **SimuScene**, a novel task and dataset for evaluating the capabilities of LLMs’ understanding, reasoning, and code-based simulation for physical scenarios, with a rigorously human-verified test set of 334 scenarios and quality-controlled training data.
2. We evaluate 10 frontier LLMs, showing even the strongest model achieves only 21% pass rate, highlighting both model limitations and the difficulty of SimuScene.
3. We propose a novel reinforcement learning approach with training signal from code-generated videos to train the underlying LLM, and demonstrate substantial improvements in simulation capabilities for smaller models. We provide a comprehensive analysis validating the reliability of our VLM-based judge and show that there is no sign of reward hacking.<sup>1</sup>

<sup>1</sup>We use AgentFly for RL training: <https://github.com/Agent-One-Lab/AgentFly>

## 2. Related Work

**Reasoning Evaluation for LLMs.** Recent research has enhanced the reasoning capabilities of LLMs by equipping them with complex thinking before generating their final response. Such LLMs include OpenAI’s o-series (OpenAI, 2024; 2025b), DeepSeek-R1, V3.1 (DeepSeek-AI, 2025; 2024), K2-Think (Cheng et al., 2025a), and Qwen3 (Qwen, 2025). As reasoning performance continues to develop, benchmarking such capabilities becomes a vital problem. Previous work has focused on math datasets, including AIME (MAA, 2024) and MATH (Hendrycks et al., 2021). Some research has focused on challenging coding tasks, such as SWE Bench (Jimenez et al., 2024) and Live-CodeBench (Jain et al., 2024). SimuScene, on the other hand, measures the novel LLM capability of generating code to simulate physical scenarios.

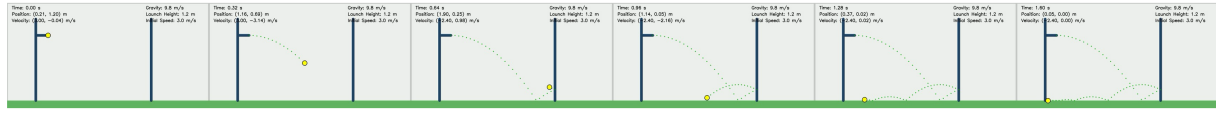
### Physical Understanding and Reasoning with LLMs

In contrast to math and code, physical understanding requires comprehending spatial relationships, temporal dynamics, and motion patterns. Early benchmarks addressed this through static attributes and plausibility judgments (e.g., elasticity, hardness, and brittleness), often framed as multiple-choice or scenario-based QA (Zellers et al., 2018; Bisk et al., 2019; Wang et al., 2023). Moving beyond static attributes, more recent benchmarks have emphasized explicit physics problem solving, ranging from undergraduate and Olympiad-level questions to robustness-focused and principle-based evaluations (Xu et al., 2025b; Yu et al., 2025; Zhang et al., 2025b; Xu et al., 2025c; Qiu et al., 2025). Other approaches integrate simulators for analysis-by-synthesis reasoning (Cherian et al., 2024). While these benchmarks provide valuable insights into textual reasoning, they stop short of validating full end-to-end simulation.

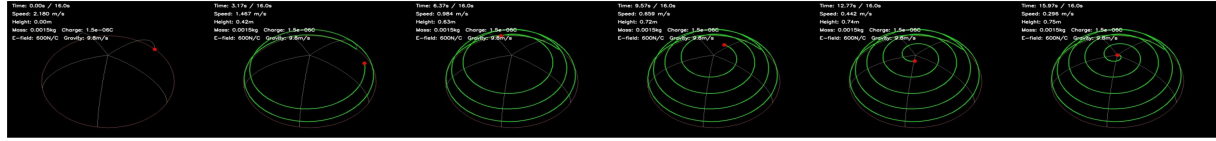
**Reinforcement Learning from Vision Signal** While reinforcement learning from vision signals has been studied in domains such as visual reasoning (Wang et al., 2024), robotics (Zitkovich et al., 2023), visual navigation (Wang et al., 2019), and embodied decision-making (Huang et al., 2025), these efforts focus on improving performance in vision-centric tasks. In LLM training, most prior work relies on verifiable ground-truth answers or an LLM to judge response quality (Cheng et al., 2025b). For our task, on the other hand, directly judging responses is not sufficient to reflect the dynamic processes in physical scenarios. We introduce the first **Code-Video-Judge** reinforcement learning paradigm, where rewards are computed by aggregating scores from multiple verification questions answered by VLMs. Our approach evaluates not only textual reasoning accuracy but also the full dynamic process through multi-question assessment.

In summary, SimuScene differs from prior work by propos-

**Mechanics:** In a controlled environment, a small, yellow, 0.18 kg ball is launched horizontally from a 1.2-meter-high wooden ramp inside a steel-framed enclosure with dimensions 2m x 1m x 1.5m. The ramp's surface has a rough texture, providing friction that limits the ball's speed to 3 m/s. The air is dry, with 20% humidity. After leaving the ramp, the ball travels for 1.6 seconds before landing on a bed of rubber pellets that absorb the impact and cause the ball to bounce slightly before settling.



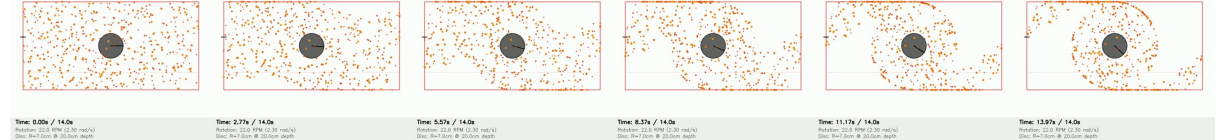
**Electromagnetism:** Inside a hemispherical dome made of clear acrylic with a diameter of 1.5 meters, a charged particle of mass 1.5 grams and charge +1.5 microcoulombs is placed at the dome's base. The dome houses a radial electric field of 600 N/C directed from the center outward. The surface inside the dome is lined with fine sandpaper to increase resistance. The humidity is maintained at 50%. When released, the particle moves along the dome's inner surface, spiraling upwards with a gradually decreasing speed due to resistance.



**Optics:** A 1.5-meter-high rectangular glass tank with a refractive index of 1.5 is filled with a vegetable oil solution. A 150-gram biconvex lens with a focal length of 22 cm and a refractive index of 1.52 is submerged horizontally at the center of the tank. A yellow LED light source is positioned directly above the lens, emitting a steady beam that refracts through the lens and oil. This setup creates a luminous yellow circle that appears on the tank's bottom, maintaining its form for over 10 seconds as the light persistently interacts with the lens and oil.



**Fluid Mechanics:** Inside a rectangular aquarium with dimensions of 100 cm by 50 cm and filled to a height of 40 cm with a transparent gel, a small stainless steel disc with a radius of 7 cm is submerged and fixed horizontally at a depth of 20 cm. The disc is rotated at a constant speed of 22 revolutions per minute by an overhead motor. The rotation of the disc generates vortices that influence the movement of suspended fine glitter particles within the gel. Over the course of 14 seconds, the glitter particles are swept into helical paths by the vortices, gradually forming concentrated, spiral formations that trace the flow patterns within the gel, showcasing the interaction of rotational motion with a semi-solid medium.



**Thermodynamics:** A light beam passes through a double convex lens inside a 75 cm high, 50 cm diameter glass cylinder filled with carbon dioxide at 1.5 atm pressure. The lens, with a refractive index of 1.55 and a focal length of 20 cm, focuses the light onto a flat black metal disk, 10 cm in diameter, located 15 cm below the lens on a roughened glass base. As the light focuses, the CO<sub>2</sub> absorbs some energy, visibly forming small, localized thermal currents in the gas above the heated disk, persisting for over 12 seconds.



Figure 1. Representative text-to-code-to-video examples from the SimuScene benchmark. Each video is rendered from LLM-generated code and illustrates the described dynamic physical process.

ing an underexplored code simulation task, VLM-as-Judge evaluation pipeline, benchmarking current LLMs, and training models with a Code-Video-Judge RL paradigm.

### 3. SimuScene

In this section, we first present the details of the **SimuScene** dataset construction, then introduce the evaluation pipeline, followed by the dataset statistics and quality analysis.

#### 3.1. Dataset Construction

**Domain Selection** Our goal is to construct a dataset that encompasses a broad range of *visualizable* dynamic physical concepts. We select five classical physics domains:

mechanics, electromagnetism, optics, fluid mechanics, and thermodynamics, due to their rich, observable motion patterns suitable for code-based simulation. Using a two-level taxonomy aligned with standard classical physics categorizations (Karaoglu, 2020), we curate 52 concepts (e.g., fluid dynamics, angular momentum, and gravity). Details are provided in Fig. 5a and § D.3.

**Scenario & Verification Question Generation** The data construction process is depicted in Fig. 2. Starting from the 52 concepts, we use GPT4o (OpenAI, 2024) to generate *basic scenarios* (e.g., “a spinning disk on a frictionless table”), and augments them with additional conditions such as collisions, external forces, or non-uniform properties, where the number of conditions

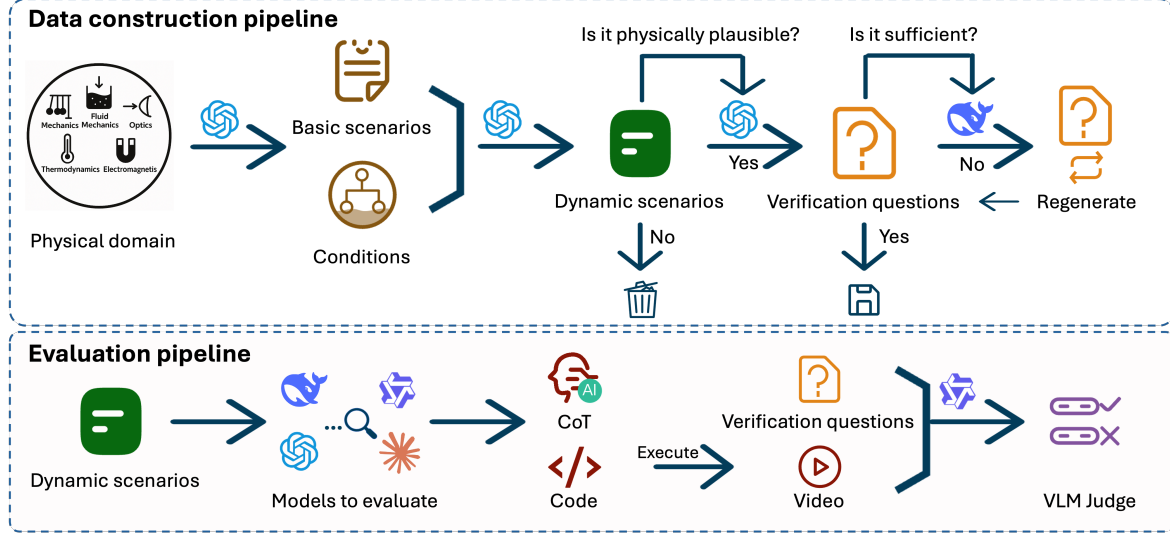


Figure 2. Overview of the SimuScene dataset construction process, including dynamic scenario and visual question generation, as well as scenario–reasoning trace–code consistency assessment.

determines the difficulty. It then evaluates each candidate scenario for physical plausibility. For these deemed valid, the model generates *visual verification questions* describing the expected motion, phrased as questions about a video that answering all as True indicates faithful representation.

**Quality Improving** To further strengthen quality control, we introduce a second layer of review: we utilize DeepSeek-R1-0528 (DeepSeek-AI, 2025) to evaluate the generated verification questions, identifying errors, ambiguities, or omissions. When issues are detected, the model revises the question to improve clarity, correctness, and completeness. This multi-step pipeline, with plausibility filtering and independent review, ensures that the resulting scenarios and verification questions meet a high standard of reliability and data integrity. Fig. 3 shows an example of the data.

**Dataset Statistics & Splits** In this way, we construct a dataset comprising 7,659 validated scenarios with their associated verification questions, of which 7,325 are allocated for training and 334 are reserved for evaluation. We ensure a minimum of four questions per concept in the test set to provide broad coverage and reduce domain or concept bias in evaluation.

For the training set, we generate eight candidate responses for each scenario using DeepSeek-R1-0528 (DeepSeek-AI, 2025). Each response is automatically annotated with a correctness label by our evaluation pipeline, which we describe in § 3.3. This procedure yields a diverse collection of model outputs paired with fine-grained correctness signals, making the dataset suitable for both supervised fine-tuning (SFT) and reinforcement learning (RL). In total, we obtain 12,556 validated responses spanning 4,182 scenarios, which

can be used for SFT. In total, we obtain 12,556 validated responses spanning 4,182 scenarios, which can be directly used for SFT, while the remaining 3,143 scenarios without valid responses can be used for RL training.

To reduce RL training difficulty and ensure sufficient warm-start, we allocate 3,000 scenarios with validated responses for supervised fine-tuning. The remaining 1,182 scenarios with valid responses are combined with 3,143 scenarios lacking valid responses for RL training, yielding 4,325 RL training scenarios. This split allows the model to learn basic patterns via SFT before tackling both solvable and challenging scenarios during RL.

Statistics including domain distribution, token lengths, and verification question counts are reported in § A.

### 3.2. Dataset Quality Control

**Human Verification of Test Set** To ensure the fidelity of the test set, we manually verified all 334 test scenarios. Each scenario was reviewed to confirm: (1) the scenario description is clear and unambiguous; (2) the scenario is plausible and can be simulated with reasonable computational resources; and (3) verification questions in each scenario cover key aspects of the motion. This rigorous human verification process ensures that our test set provides a reliable benchmark for evaluating LLM-generated simulations.

**Training Data Quality Inspection** To assess the quality of our automatically-generated training data, we conducted manual inspection on randomly-sampled subsets: 50 examples from the SFT training data and 50 examples from the RL training data. For each sample, annotators evaluated: (1) whether the scenario description is clear and unambiguous;

<b>Domain:</b> Electromagnetism	<b>Concept:</b> Electric Potential
<b>Basic Scenario:</b> A charged particle performs <b>spiral motion</b> in an electric field.	
<b>Conditions:</b> 1. Introducing <b>conductors of different shapes</b> to change the electric field distribution; 2. Including <b>surface resistance or friction</b> to gradually dissipate the particle’s kinetic energy.	
<b>Dynamic Scenario:</b> Inside a <b>hemispherical dome</b> made of clear acrylic with diameter <b>1.5m</b> , a charged particle of mass <b>1.5g</b> and charge <b>+1.5<math>\mu</math>C</b> is placed at the dome’s base. The dome houses a radial electric field of <b>600N/C</b> directed from center outward. Surface lined with fine sandpaper for resistance. Humidity: <b>50%</b> . When released, particle moves along dome’s inner surface, <b>spiraling upwards</b> with <b>gradually decreasing speed</b> due to resistance.	
<b>Verification Questions:</b> 1. A <b>hemispherical dome</b> is present as container; 2. A <b>charged particle</b> is initially placed at dome’s base; 3. Charged particle moves along <b>inner surface</b> of dome; 4. Particle moves in <b>spiraling trajectory</b> ; 5. Particle’s <b>speed visibly decreases</b> as it spirals upwards; 6. Particle takes <b>visible time</b> to reach top; 7. Particle <b>reaches the top</b> of dome after motion.	

Figure 3. Examples from SimuScene. A corresponding video is shown as the second entry in Fig. 1.

ous; (2) whether the scenario is physically plausible and can be reasonably simulated; and (3) whether the verification questions adequately capture the key motion characteristics.

The results show that 88.5% of SFT samples and 80.0% of RL samples meet our quality standards, demonstrating the robustness of our automated data construction pipeline. Manual inspection revealed that the main issues stem from ambiguous physical descriptions and incomplete verification coverage. The slightly lower quality rate for RL data is expected and reasonable: SFT data underwent VLM-based filtering to retain only correct examples, whereas RL data intentionally includes both successful and failed attempts to provide diverse training signal for reinforcement learning.

### 3.3. Evaluation Pipeline

**Code–Video–VLM Evaluation** We propose a novel evaluation pipeline for assessing LLM-generated simulations, which consists of three steps: (i) *Code Generation*. First, the tested LLM is given a scenario description together with an instruction prompt that asks it to generate Python code simulating the scenario. The prompt specifies key details such as how to represent objects, the duration of the video, and the requirement to save the output in MP4 format (the exact prompt is shown in § K). (ii) *Video Rendering*. Then, we collect the model’s responses, extract the Python code enclosed in Python code blocks, and execute it to render videos depicting the corresponding dynamic motions. (iii) *VLM-based Verification*. Finally, we feed the generated videos, along with the scenario description and associated verification questions, into a vision-language model.<sup>2</sup> We prompt it to answer each verification question with true or false. A response is judged consistent with the scenario if all answers are true. More visualized examples of VLM judgments, including both consistent and inconsistent cases,

<sup>2</sup>We compared several open-source vision–language models on our task and found that Qwen-2.5-72B-VL achieved the most accurate judgments.

Table 1. Agreement rates between VLM and human annotators.

Model	Agreement (%)
Qwen2.5-VL-72B-Instruct (Team, 2024)	87.8
Qwen3-VL-235B-A22B-Instruct (Bai et al., 2025)	84.3
InternVL-3.5 (Wang et al., 2025b)	83.4
GLM-4.6V (Team et al., 2025)	84.5

are provided in § G.

**Validation of Evaluation Reliability** To validate the effectiveness of our proposed pipeline, we conducted comprehensive human evaluation on our test set. We fed the test set to DeepSeek-R1-0528 (DeepSeek-AI, 2025) with 8 responses per sample, yielding 2,672 responses in total, of which 2,142 videos were successfully rendered. Two independent annotators evaluated these videos, achieving an inter-annotator agreement of 87%, indicating strong consistency. After resolving disagreements through discussion, the final human labels were established.

We then compared these human labels against the outputs of our VLM judges. Table 1 reports the agreement rates between each VLM and human annotations. Qwen2.5-VL-72B-Instruct (Team, 2024) achieves the highest agreement, and all models have agreement rates above 83%, demonstrating the reliability of VLM-based evaluation for our task. A more detailed error analysis is shown in § C.

## 4. Evaluation of Frontier LLMs

We evaluate a series of contemporary reasoning models, including open-source models — GPT-oss (20B, 120B) (OpenAI, 2025), Qwen3 (32B, 235B-A22B) (Qwen, 2025), Deepseek-R1-0528 (DeepSeek-AI, 2025) and Deepseek-V3.1 (671B) (DeepSeek-AI, 2024) — as well as the proprietary models — Gemini-2.5-pro (Comanici et al., 2025), GPT-o3, GPT-o4-mini, and GPT-5 (OpenAI, 2025b;a). We use the evaluation protocol described in § 3.3.

Table 2. Comparison of frontier LLMs on the SimuPhy benchmark. Metrics include Executable Rate (E.R.), Render Rate (R.R.), Playable Rate (P.R.), and VLM-evaluated Accuracy (Acc.). Avg@8 reports average performance across 8 runs, while Pass@8 evaluates at the scenario level, where a scenario is considered correct if at least one of the 8 responses yields a valid solution.

Model	Size	Avg@8				Pass@8			
		E.R.	R.R.	P.R.	Acc.	E.R.	R.R.	P.R.	Acc.
Gemini-2.5-pro (Comanici et al., 2025)	-	99.1	77.3	38.0	12.7	100.0	99.7	77.8	37.4
GPT-o3 (OpenAI, 2025b)	-	98.9	75.2	64.1	15.9	100.0	100.0	95.5	45.2
GPT-o4-mini (OpenAI, 2025b)	-	88.1	86.9	78.6	17.2	100.0	100.0	95.5	42.5
GPT-5-medium (OpenAI, 2025a)	-	97.2	68.9	55.7	20.5	100.0	100.0	93.1	59.9
GPT-oss-20b (OpenAI, 2025)	21.5B	99.1	92.0	61.6	10.5	100.0	100.0	85.6	32.0
GPT-oss-120b (OpenAI, 2025)	120B	99.8	93.7	76.0	14.0	100.0	99.7	91.9	37.4
Qwen3-32B (Qwen, 2025)	32B	99.8	96.6	51.0	11.1	100.0	100.0	82.6	30.5
Qwen3-235B-A22B (Qwen, 2025)	235B	99.7	95.9	68.5	15.1	100.0	100.0	91.3	41.0
DeepSeek-R1-0528 (DeepSeek-AI, 2025)	671B	99.7	97.3	77.0	21.5	100.0	100.0	93.4	52.7
DeepSeek-V3.1(DeepSeek-AI, 2024)	671B	99.9	95.2	64.0	14.5	100.0	99.4	90.4	40.7

#### 4.1. Metrics

Based on the evaluation process, we designed the following evaluation metrics, all of which are computed over all generated responses.

- **Executable Rate (E.R.)** The percentage of generated code that is executable.
- **Render Rate (R.R.)** The percentage of generated code that successfully renders videos.
- **Playable Rate (P.R.)** The percentage of generated code that results in a playable video.
- **Accuracy (Acc.)** The percentage of outputs that are evaluated as passing by our proposed multiple-question VLM-as-a-judge method. This is the primary metric, measuring the end-to-end performance of LLMs, which combines physical understanding, reasoning, and code simulation.

Table. 2 summarizes the results of the LLMs on SimuScene. We report Avg@8 and Pass@8 to assess both the average performance of model outputs, and their best-case capability. To thoroughly explore model capabilities during evaluation, we employ a carefully designed complex prompt (detailed in § K), whereas our training uses simpler prompts to ensure better generalization. All models are evaluated under their default configurations; unless otherwise specified, results correspond to the thinking mode, while entries marked with \* indicate non-thinking mode. As shown in the table, several performance patterns emerge across executability, renderability, playability, and end-to-end accuracy.

**Low end-to-end performance highlights task difficulty.** All models achieve very low performance in end-to-end evaluation, highlighting their limited ability to comprehensively understand dynamic physical scenes and translate it into code simulations. Notably, even the strongest model,

Table 3. DeepSeek-R1-0528 performance breakdown across domains.

Category	Avg@8	Pass@8
Mechanics	27.7	58.8
Electromagnetism	20.8	60.0
Optics	8.4	27.0
Fluid Mechanics	20.5	50.0
Thermodynamics	26.0	80.0

DeepSeek-R1-0528, achieves only 21.5% Avg@8 accuracy. This underscores the exceptional difficulty of our benchmark and reveals significant gaps in the scene simulation capabilities of modern LLMs.

**High code generation capability but weak scene alignment.** Most models achieve high executable rate (E.R.) and render rate (R.R), showing they can generate bug-free code that produces videos. However, lower playable rate (P.R.) and accuracy (ACC.) indicate persistent difficulties in correctly translating scene descriptions into aligned visual simulations and faithful motion dynamics.

**Pass@8 reveals hidden potential.** While Avg@8 scores are low across all models, Pass@8 metrics show substantially higher success rates, with the best models approaching 60%. This large gap between Avg@8 and Pass@8 indicates that current models have potential to generate correct simulations but lack the consistency to do so reliably.

To better understand the difficulty of SimuScene across domains, we present in Table. 3 a domain-level breakdown of DeepSeek-R1-0528’s performance. The results show marked variation across domains. The model performs strongest on mechanics and thermodynamics, achieving 27.7% Avg@8 in mechanics and 80.0% Pass@8 in thermo-

dynamics. By contrast, optics emerges as the most challenging domain, with only 8.4% Avg@8 and 27.0% Pass@8, likely reflecting the scarcity of optics-related supervision during training. Nevertheless, the low Avg@8 scores across all domains highlight the fundamental difficulty of the task.

## 5. Model Training for Better Code Simulation

In this section, we present experiments and results for the proposed training approach, which applies supervised finetuning (SFT) followed by reinforcement learning (RL) with a vision-based reward signal using the curated training data. § 5.1 describes the experimental setup and § 5.2 introduces the reward design, while § 5.3 presents the main results for training, § 5.5 provides discussion and analysis of reward hacking, § 5.6 discusses mixing our data with general reasoning data.

### 5.1. Experimental Setup

For supervised finetuning, we use the data with passed responses mentioned in § 3 to finetune DeepSeek-R1-Distill-Qwen-7B and Qwen3-32B. We use the AdamW optimizer, with maximum learning rate set to  $4 \times 10^{-5}$  and linearly scaled to 0. We train the model for 2 epochs with a batch size of 256. During training, all samples are truncated to a maximum of 16,384 tokens. The training takes about 32 GPU hours in total.

For reinforcement learning, we adopt GRPO (Shao et al., 2024) to aggregate reward implemented on top of the Agent-Fly (Wang et al., 2025a) (more training details in § D.1). We use the Adam optimizer with a learning rate of  $5 \times 10^{-7}$ , train for 150 steps with a global train batch size of 32 and 8 rollouts per sample, totaling 576 GPU-hours. All rollouts are truncated to a maximum of 16,384 tokens.

### 5.2. Code-Video-Judge Reward Design

Each sample scenario  $s$  in our dataset is paired with a set of verification questions  $\mathcal{Q} = \{q_i\}_{i=1}^M$ , designed to test whether the response matches the physical scenarios. For each  $q_i$ , the VLM yields a binary label  $y_i \in \{\text{TRUE}, \text{FALSE}\}$ . If compilation or execution fails, resulting in an unusable video, we set  $\tilde{y}_i = \text{FALSE}$  for all  $i$ . Otherwise we use the following reward:

$$r_{binary} = \mathbf{1}[\tilde{y}_i = \text{TRUE} \text{ for all } i \text{ in } M] \quad (1)$$

Here  $r_{binary}$  is a binary reward such that all verification questions must be answered with TRUE to get a value of 1.0.

### 5.3. Main Results

We report results for *DeepSeek-R1-Distill-Qwen-7B* and *Qwen3-32B* trained with our SFT and RL pipelines. Unless

Table 4. Performance of DeepSeek-R1-Distill-Qwen-7B and Qwen3-32B across three stages: base model, after SFT, and after RL with different reward signals.

Model	Avg@8				Pass@8			
	E.R.	R.R.	P.R.	Acc.	E.R.	R.R.	P.R.	Acc.
Base Model (7B)	62.1	2.3	0.2	0.0	99.1	10.5	1.8	0.0
w/ SFT	93.8	87.1	30.0	4.4	100.0	100.0	72.8	18.3
w/ RL	99.1	98.1	81.5	11.1	100.0	100.0	95.2	34.4
Base Model (32B)	99.8	96.6	51.0	11.1	100.0	100.0	82.6	30.5
w/ SFT	97.7	95.3	74.3	17.4	100.0	100.0	92.0	43.1
w/ RL	99.9	97.7	90.6	36.9	100.0	100.0	98.5	72.2

otherwise stated, we use the VLM-as-judge binary reward  $r_{binary}$  as the default. Overall results are summarized in Table 4. The base model does not perform well on end-to-end simulation, while SFT improves all metrics substantially.

Compared to a model trained only with SFT, adding RL boosts the render-to-play conversion (P.R./R.R.). In practice, this means that most rendered videos become playable, showing that RL improves runtime reliability and pipeline assembly. In terms of Pass@8, under RL, performance approaches saturation with E.R. = 100.0%, R.R. = 100.0%, and P.R. = 95.2%, while Acc. rises from 18.3% to 34.4% for a gain of about 1.8×.

With our training, the 7B model attains a Pass@8 accuracy of **34.4%**, which is comparable to that of several substantially larger models. And the 32B model even achieves the best performance of (Pass@8 **72.2%**), surpassing best untrained models like DeepSeek-R1. This result indicates that targeted data curation and training can meaningfully improve performance on scenario-consistent simulation. Taken together, the observed gains support the usefulness of our dataset design, training procedure, and vision-based reward signal, while also suggesting that further improvements remain possible.

### 5.4. Reward Variants

We compare the proposed reward against two alternative variants, using the same set of verification questions. The first variant employs *VLM-as-judge*, but defines the reward as the fraction of correctly verified questions, yielding a score between 0 and 1, as follows:

$$r_{ratio} = \frac{1}{M} \sum_{i=1}^M \mathbf{1}[\tilde{y}_i = \text{TRUE}] \quad (2)$$

The second variant uses *LLM-as-judge* (text-only), where the verification questions are replaced with direct judgments of the generated code. Further details are provided in § E.2. Training curves are depicted in Fig. 4.

As shown by the reward trajectories in Fig. 4, all the three judges yield steadily improving signals during RL. Although *VLM-as-judge* variants does not achieve larger reward scores

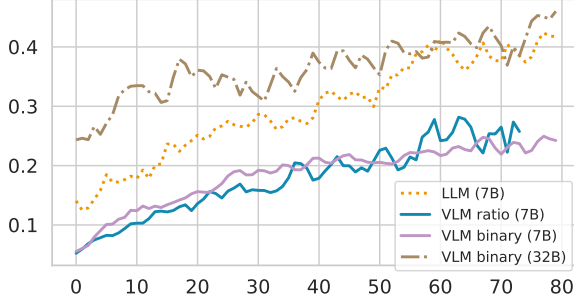


Figure 4. The reward curve during RL training. All four rewards yield steadily improving signals.

than the *LLM-as-judge*, they show better simulation performance. This indicates that using VLMs achieves more faithful rewards and better consistency compared to LLMs. And we deduct that this gap arises from two sources. (i) **Modality fidelity.** VLMs evaluate rendered videos, directly observing motion and interactions, whereas text-only LLMs must infer runtime behavior from static code, leading to optimistic false positives for physically implausible or visually invalid outcomes. (ii) **Execution observability.** Our pipeline assigns zero reward to compilation or execution failures, tightly coupling VLM rewards to end-to-end reliability. In contrast, text-only judges do not execute code and can be exploited by superficially valid but non-rendering code.

As a result, visual feedback closes the loop from code to video and verification, aligning the reward with the end-to-end objective, and reducing reliance on spurious textual cues. Response length trends are reported in § F.

### 5.5. Discussion and Reward Hacking

Reward hacking refers to the policy exploiting biases, artifacts, or loopholes in the reward function to achieve high rewards without genuinely improving on the true objective. Since we use VLMs to judge videos, we discuss our effort to prevent reward hacking, and perform manual checks to ensure it is not likely to happen during our training.

**Preventing Reward Hacking** We employ three key design strategies to mitigate reward hacking: (1) *Multi-Question Aggregated Rewards*. Unlike binary pass/fail rewards that provide a single scalar signal per scenario, our approach evaluates multiple verification questions (4–12 per scenario) and aggregates their individual scores. This design makes it substantially harder for the policy to exploit reward biases. (2) *Ensemble VLM Voting During Training*. We use three different vision-language models (Qwen3-VL-235B (Bai et al., 2025), InternVL3.5 (Wang et al., 2025b), GLM-4.6V (Team et al., 2025)) to evaluate each generated video during training, with majority voting determining the final reward. (3)

Table 5. Performance on math, code, and physical reasoning by mixing SFT dataset with OpenThoughts (OT) 10k examples. We measure performance on three domains: math (AIME24, AIME25), coding (HumanEval+, MBPP+), and physics reasoning (UGPhysics, PhysReason).

Task	AIME24	AIME25	HumanEval+	MBPP+	UGPhysics	PhysReason
Base	46.67	35.26	39.02	35.71	16.68	43.27
w/ Ours	32.24	25.05	52.44	32.28	11.13	36.17
w/ OT	46.61	32.97	7.93	11.64	12.67	39.20
w/ Ours + OT	46.15	33.13	60.37	45.77	12.73	38.74

**Train-Test VLM Separation.** Critically, we use a different VLM for evaluation (Qwen2.5-VL-72B-Instruct) than those used during training (Qwen3-VL, InternVL3.5, GLM-4.6V). This separation creates a strong test of generalization: if the policy has learned to exploit specific biases of the training VLMs, it would fail when evaluated by a different model. Given that our trained models exhibit are substantially worse than large models provides evidence against systematic reward hacking.

**Empirical Validation Through Human Evaluation.** To rigorously verify that our RL-trained models achieve genuine improvements rather than exploiting VLM biases, we conduct human evaluation on model outputs after RL training. After verifying all scenarios in the test set, we observe an agreement rate of 86.9% between human judgments and VLM evaluations, suggesting no clear evidence of systematic reward hacking under our training setup. Fig. 10 compares model performance before and after RL.

### 5.6. Dataset Mixing

Finally, to understand how training with our dataset affects other capabilities, we mix our SFT dataset with OpenThoughts, a general reasoning dataset covering math, science, code, and puzzles (Guha et al., 2025), and analyze the performance on data mixture. We use the full set of our SFT dataset and 10k examples from OpenThoughts. Results are shown in Table 5. We measure performance on math (AIME (MAA, 2024)), coding (HumanEval+ and MBPP+ (Liu et al., 2023)), and physics reasoning (UGPhysics (Xu et al., 2025a) and PhysReason (Zhang et al., 2025a)).

When using our SFT data alone, there is a small drop in math and physics reasoning performance, but slight improvement in coding. This is expected since responses in our data are mainly code. However, when mixing our data with general reasoning data, there is a large improvement in the code domain, while the performance in math and physics is maintained. This indicates that our dataset can be used in general-purpose training, improving code simulation while not interfering with performance in other domains.

## 6. Conclusion

We introduced SimuScene, a new task and benchmark that evaluates whether LLMs can understand, reason about, and simulate physical scenarios through code generation. We built a fully automatic construction pipeline that (*i*) generates topic-conditioned dynamic scenarios and visual verification questions, (*ii*) produces reasoning traces and executable code, and (*iii*) validates rendered videos via a VLM. The resulting dataset contains 7,649 scenarios across five physics domains, with a 334-example human-verified test set; VLM judgements show 87.8% agreement with human labels, supporting their use as reliable evaluators. Results for contemporary LLMs reveal that the task is challenging: even frontier models attain only modest accuracy under Avg@8, which highlights gaps in current physical-law reasoning. Building on SimuScene, we employ reinforcement learning with verifiable rewards (RLVR) coupled with SFT, which substantially improves end-to-end text to code to video consistency.

## Impact Statement

This paper presents work whose goal is to advance the field of machine learning by improving the ability of LLMs to understand and simulate physical scenarios through code generation. Our work has potential positive societal impacts, particularly in education, by enabling automated generation of physics simulations that can make complex concepts more accessible to students worldwide. The benchmark can also guide the development and evaluation of model capabilities in this domain. However, we acknowledge potential risks: generated simulations, while educational, may contain subtle inaccuracies that could mislead users if treated as scientifically-precise models rather than educational tools. Additionally, our reliance on VLM-based evaluation, though validated against human judgment, introduces dependencies on vision-language model capabilities and potential biases. We encourage responsible use of our dataset and methods with appropriate validation in educational or scientific contexts. Overall, we believe the educational benefits and contributions to physical reasoning capabilities outweigh the risks when used appropriately.

## References

Bai, S., Cai, Y., Chen, R., Chen, K., Chen, X., Cheng, Z., Deng, L., Ding, W., Gao, C., Ge, C., Ge, W., Guo, Z., Huang, Q., Huang, J., Huang, F., Hui, B., Jiang, S., Li, Z., Li, M., Li, M., Li, K., Lin, Z., Lin, J., Liu, X., Liu, J., Liu, C., Liu, Y., Liu, D., Liu, S., Lu, D., Luo, R., Lv, C., Men, R., Meng, L., Ren, X., Ren, X., Song, S., Sun, Y., Tang, J., Tu, J., Wan, J., Wang, P., Wang, P., Wang, Q., Wang, Y., Xie, T., Xu, Y., Xu, H., Xu, J., Yang, Z., Yang, M.,

Yang, J., Yang, A., Yu, B., Zhang, F., Zhang, H., Zhang, X., Zheng, B., Zhong, H., Zhou, J., Zhou, F., Zhou, J., Zhu, Y., and Zhu, K. Qwen3-vl technical report, 2025. URL <https://arxiv.org/abs/2511.21631>.

Bisk, Y., Zellers, R., Bras, R. L., Gao, J., and Choi, Y. Piqa: Reasoning about physical commonsense in natural language, 2019. URL <https://arxiv.org/abs/1911.11641>.

Cheng, Z., Fan, R., Hao, S., Killian, T. W., Li, H., Sun, S., Ren, H., Moreno, A., Zhang, D., Zhong, T., Xiong, Y., Hu, Y., Xie, Y., Han, X., Wang, Y., Pimpalkhute, V., Zhuang, Y., Singh, A., Liang, X., Xie, A., She, J., Fan, D., Gao, C., Ma, L., Yurochkin, M., Maggs, J., Ma, X., He, G., Hu, Z., Liu, Z., and Xing, E. P. K2-think: A parameter-efficient reasoning system, 2025a. URL <https://arxiv.org/abs/2509.07604>.

Cheng, Z., Hao, S., Liu, T., Zhou, F., Xie, Y., Yao, F., Bian, Y., Zhuang, Y., Dey, N., Zha, Y., Gu, Y., Zhou, K., Wang, Y., Li, Y., Fan, R., She, J., Gao, C., Saparov, A., Li, H., Killian, T. W., Yurochkin, M., Liu, Z., Xing, E. P., and Hu, Z. Revisiting reinforcement learning for llm reasoning from a cross-domain perspective, 2025b. URL <https://arxiv.org/abs/2506.14965>.

Cherian, A., Corcodel, R., Jain, S., and Romeres, D. Llmphy: Complex physical reasoning using large language models and world models, 2024. URL <https://arxiv.org/abs/2411.08027>.

Chow, W., Mao, J., Li, B., Seita, D., Guizilini, V., and Wang, Y. Physbench: Benchmarking and enhancing vision-language models for physical world understanding, 2025. URL <https://arxiv.org/abs/2501.16411>.

Comanici, G., Bieber, E., Schaekermann, M., Pasupat, I., Sachdeva, N., Dhillon, I., Blistein, M., Ram, O., Zhang, D., Rosen, E., et al. Gemini 2.5: Pushing the frontier with advanced reasoning, multimodality, long context, and next generation agentic capabilities. *arXiv preprint arXiv:2507.06261*, 2025.

DeepSeek-AI. Deepseek-v3 technical report, 2024. URL <https://arxiv.org/abs/2412.19437>.

DeepSeek-AI. Deepseek-r1: Incentivizing reasoning capability in llms via reinforcement learning, 2025. URL <https://arxiv.org/abs/2501.12948>.

Guha, E., Marten, R., Keh, S., Raoof, N., Smyrnis, G., Bansal, H., Nezhurina, M., Mercat, J., Vu, T., Sprague, Z., et al. Openthoughts: Data recipes for reasoning models. *arXiv preprint arXiv:2506.04178*, 2025.

Hendrycks, D., Burns, C., Kadavath, S., Arora, A., Basart, S., Tang, E., Song, D., and Steinhardt, J. Measuring mathematical problem solving with the math dataset. *NeurIPS*, 2021.

Huang, Z., Sheng, Z., Qu, Y., You, J., and Chen, S. Vlm-rl: A unified vision language models and reinforcement learning framework for safe autonomous driving. *Transportation Research Part C: Emerging Technologies*, 180: 105321, 2025.

Jain, N., Han, K., Gu, A., Li, W.-D., Yan, F., Zhang, T., Wang, S., Solar-Lezama, A., Sen, K., and Stoica, I. Livecodebench: Holistic and contamination free evaluation of large language models for code. *arXiv preprint arXiv:2403.07974*, 2024.

Jimenez, C. E., Yang, J., Wettig, A., Yao, S., Pei, K., Press, O., and Narasimhan, K. R. SWE-bench: Can language models resolve real-world github issues? In *The Twelfth International Conference on Learning Representations*, 2024. URL <https://openreview.net/forum?id=VTF8yNQM66>.

Karaoglu, B. *Classical Physics: A Two-Semester Coursebook*. Springer International Publishing, 2020. ISBN 9783030384562. URL <https://books.google.ae/books?id=1ZHTDwAAQBAJ>.

Liu, J., Xia, C. S., Wang, Y., and Zhang, L. Is your code generated by chatGPT really correct? rigorous evaluation of large language models for code generation. In *Thirty-seventh Conference on Neural Information Processing Systems*, 2023. URL <https://openreview.net/forum?id=1qvx610Cu7>.

Luo, Z., Shen, Z., Yang, W., Zhao, Z., Jwalapuram, P., Saha, A., Sahoo, D., Savarese, S., Xiong, C., and Li, J. Mcp-universe: Benchmarking large language models with real-world model context protocol servers. *arXiv preprint arXiv:2508.14704*, 2025.

MAA. American invitational mathematics examination (aime), 2024. URL <https://maa.org/math-competitions/american-invitational-mathematics-examination-aime>.

Merrill, M. A., Shaw, A. G., Carlini, N., Li, B., Raj, H., Bercovich, I., Shi, L., Shin, J. Y., Walshe, T., Buchanan, E. K., et al. Terminal-bench: Benchmarking agents on hard, realistic tasks in command line interfaces. *arXiv preprint arXiv:2601.11868*, 2026.

OpenAI. Gpt-4o system card, 2024. URL <https://arxiv.org/abs/2410.21276>.

OpenAI. o1 — openai api documentation. <https://platform.openai.com/docs/models/o1>, 2024.

OpenAI. gpt-oss-120b & gpt-oss-20b model card, 2025. URL <https://arxiv.org/abs/2508.10925>.

OpenAI. GPT-5-medium. <https://platform.openai.com/models>, 2025a. Large language model.

OpenAI. Introducing OpenAI o3 and o4-mini. <https://openai.com/index/introducing-o3-and-o4-mini/>, 2025b. URL <https://openai.com/index/introducing-o3-and-o4-mini/>.

Qiu, S., Guo, S., Song, Z.-Y., Sun, Y., Cai, Z., Wei, J., Luo, T., Yin, Y., Zhang, H., Hu, Y., Wang, C., Tang, C., Chang, H., Liu, Q., Zhou, Z., Zhang, T., Zhang, J., Liu, Z., Li, M., Zhang, Y., Jing, B., Yin, X., Ren, Y., Fu, Z., Ji, J., Wang, W., Tian, X., Lv, A., Man, L., Li, J., Tao, F., Sun, Q., Liang, Z., Mu, Y., Li, Z., Zhang, J.-J., Zhang, S., Li, X., Xia, X., Lin, J., Shen, Z., Chen, J., Xiong, Q., Wang, B., Wang, F., Ni, Z., Zhang, B., Cui, F., Shao, C., Cao, Q.-H., xing Luo, M., Yang, Y., Zhang, M., and Zhu, H. X. Phybench: Holistic evaluation of physical perception and reasoning in large language models, 2025. URL <https://arxiv.org/abs/2504.16074>.

Qwen. Qwen3 technical report, 2025. URL <https://arxiv.org/abs/2505.09388>.

Shao, Z., Wang, P., Zhu, Q., Xu, R., Song, J., Bi, X., Zhang, H., Zhang, M., Li, Y. K., Wu, Y., and Guo, D. Deepseekmath: Pushing the limits of mathematical reasoning in open language models, 2024. URL <https://arxiv.org/abs/2402.03300>.

Team, Q. Qwen2.5: A party of foundation models, September 2024. URL <https://qwenlm.github.io/blog/qwen2.5/>.

Team, Q. Qwen2.5-vl, January 2025. URL <https://qwenlm.github.io/blog/qwen2.5-vl/>.

Team, V., Hong, W., Yu, W., Gu, X., Wang, G., Gan, G., Tang, H., Cheng, J., Qi, J., Ji, J., Pan, L., Duan, S., Wang, W., Wang, Y., Cheng, Y., He, Z., Su, Z., Yang, Z., Pan, Z., Zeng, A., Wang, B., Chen, B., Shi, B., Pang, C., Zhang, C., Yin, D., Yang, F., Chen, G., Xu, J., Zhu, J., Chen, J., Chen, J., Chen, J., Lin, J., Wang, J., Chen, J., Lei, L., Gong, L., Pan, L., Liu, M., Xu, M., Zhang, M., Zheng, Q., Yang, S., Zhong, S., Huang, S., Zhao, S., Xue, S., Tu, S., Meng, S., Zhang, T., Luo, T., Hao, T., Tong, T., Li, W., Jia, W., Liu, X., Zhang, X., Lyu, X., Fan, X., Huang, X., Wang, Y., Xue, Y., Wang, Y., Wang, Y., An, Y., Du, Y., Shi, Y., Huang, Y., Niu, Y., Wang, Y., Yue, Y., Li, Y., Zhang, Y., Wang, Y., Wang, Y., Zhang, Y., Xue, Z., Hou, Z., Du, Z., Wang, Z., Zhang, P., Liu, D., Xu, B., Li, J., Huang, M., Dong, Y., and Tang, J. Glm-4.5v and glm-4.1v-thinking: Towards versatile multimodal reasoning with scalable reinforcement learning, 2025. URL <https://arxiv.org/abs/2507.01006>.

Wang, R., Genadi, R. A., Bouardi, B. E., Wang, Y., Koto, F., Liu, Z., Baldwin, T., and Li, H. Agentfly: Extensible and scalable reinforcement learning for lm agents. *arXiv preprint arXiv:2507.14897*, 2025a.

Wang, W., Gao, Z., Gu, L., Pu, H., Cui, L., Wei, X., Liu, Z., Jing, L., Ye, S., Shao, J., et al. Internvl3.5: Advancing open-source multimodal models in versatility, reasoning, and efficiency. *arXiv preprint arXiv:2508.18265*, 2025b.

Wang, X., Huang, Q., Celikyilmaz, A., Gao, J., Shen, D., Wang, Y.-F., Wang, W. Y., and Zhang, L. Reinforced cross-modal matching and self-supervised imitation learning for vision-language navigation. In *Proceedings of the IEEE/CVF conference on computer vision and pattern recognition*, pp. 6629–6638, 2019.

Wang, Y., Cao, M., Lin, H., Han, M., Ma, L., Jiang, J., Cheng, Y., and Liang, X. Eaco: Enhancing alignment in multimodal llms via critical observation. *arXiv preprint arXiv:2412.04903*, 2024.

Wang, Y. R., Duan, J., Fox, D., and Srinivasa, S. Newton: Are large language models capable of physical reasoning?, 2023. URL <https://arxiv.org/abs/2310.07018>.

Xiang, K., Li, H., Zhang, T. J., Huang, Y., Liu, Z., Qu, P., He, J., Chen, J., Yuan, Y.-J., Han, J., Xu, H., Li, H., Sachan, M., and Liang, X. Seephys: Does seeing help thinking? – benchmarking vision-based physics reasoning, 2025. URL <https://arxiv.org/abs/2505.19099>.

Xu, X., Xu, Q., Xiao, T., Chen, T., Yan, Y., Zhang, J., Diao, S., Yang, C., and Wang, Y. Ugphysics: A comprehensive benchmark for undergraduate physics reasoning with large language models. *arXiv preprint arXiv:2502.00334*, 2025a.

Xu, X., Xu, Q., Xiao, T., Chen, T., Yan, Y., Zhang, J., Diao, S., Yang, C., and Wang, Y. Ugphysics: A comprehensive benchmark for undergraduate physics reasoning with large language models, 2025b. URL <https://arxiv.org/abs/2502.00334>.

Xu, Y., Liu, Y., Gao, Z., Peng, C., and Luo, D. Physense: Principle-based physics reasoning benchmarking for large language models, 2025c. URL <https://arxiv.org/abs/2505.24823>.

Yu, F., Wan, H., Cheng, Q., Zhang, Y., Chen, J., Han, F., Wu, Y., Yao, J., Hu, R., Ding, N., Cheng, Y., Chen, T., Bai, L., Zhou, D., Luo, Y., Cui, G., and Ye, P. Hiphoto: How far are (m)llms from humans in the latest high school physics olympiad benchmark?, 2025. URL <https://arxiv.org/abs/2509.07894>.

Zellers, R., Bisk, Y., Schwartz, R., and Choi, Y. Swag: A large-scale adversarial dataset for grounded commonsense inference, 2018. URL <https://arxiv.org/abs/1808.05326>.

Zhang, X., Dong, Y., Wu, Y., Huang, J., Jia, C., Fernando, B., Shou, M. Z., Zhang, L., and Liu, J. Physreason: A comprehensive benchmark towards physics-based reasoning. *arXiv preprint arXiv:2502.12054*, 2025a.

Zhang, Y., Ma, Y., Gu, Y., Yang, Z., Zhuang, Y., Wang, F., Huang, Z., Wang, Y., Huang, C., Song, B., Lin, C., and Zhao, J. Abench-physics: Benchmarking physical reasoning in llms via high-difficulty and dynamic physics problems, 2025b. URL <https://arxiv.org/abs/2507.04766>.

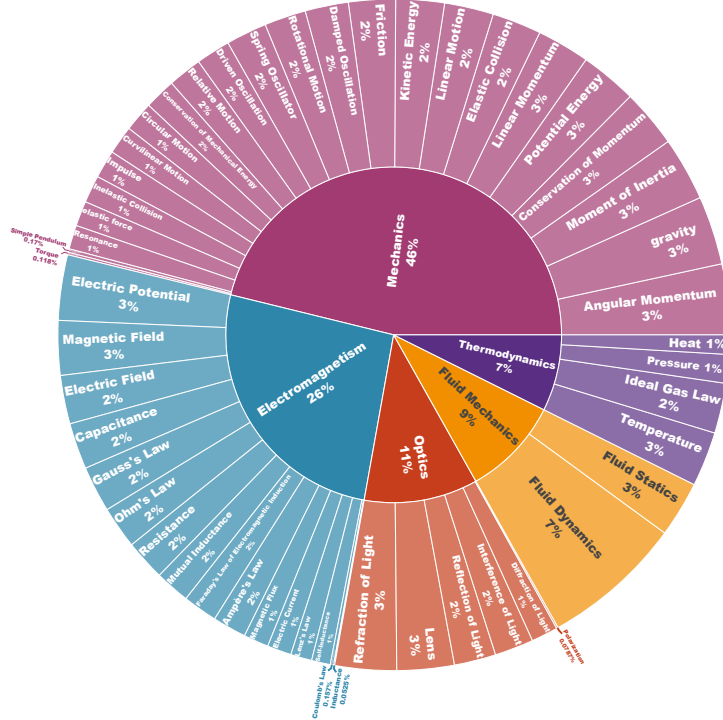
Zitkovich, B., Yu, T., Xu, S., Xu, P., Xiao, T., Xia, F., Wu, J., Wohlhart, P., Welker, S., Wahid, A., et al. Rt-2: Vision-language-action models transfer web knowledge to robotic control. In *Conference on Robot Learning*, pp. 2165–2183. PMLR, 2023.

## A. Analysis of Dataset Properties

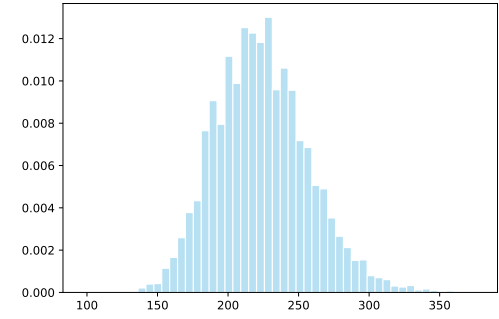
In this section, we analyze the properties of the **SimuScene** dataset, including domain distribution, token length distribution, and VLM verification counts.

**Domain Distribution.** Among the five general domains (Fig. 5a), mechanics includes 24 core concepts and electromagnetism includes 16, together comprising the majority of the dataset. The remaining three domains account for only 12 core concepts in total. We focus on mechanics and electromagnetism because their concepts are more common in daily life and generally easier to understand and visualize.

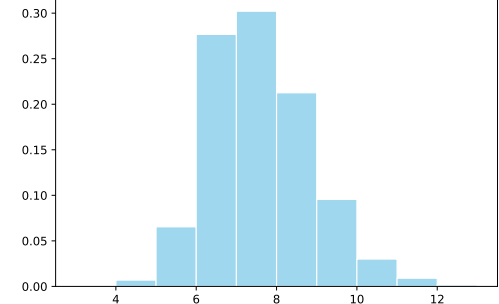
**Scenario Length and Question Count.** Beyond domains, we examine both the length of generated scenarios and the number of associated verification questions. Using the Qwen3 tokenizer (Fig. 5b), scenario lengths range from 100 to 350 tokens, with a near-normal distribution centered around 225, suggesting moderate complexity while avoiding extremes of brevity or verbosity. For verification questions (Fig. 5c), each scenario yields between 4 and 12, most often 6 to 10, which offers sufficient coverage of the motion process without redundancy while preserving scalability across varying levels of complexity.



(a) Topic distribution of generated scenario across physics domains. Inner ring: domains; outer ring: concepts. Labels show the percentages.



(b) Token count distribution per scenario in SimuScene, measured using the Qwen3 tokenizer.



(c) VLM verification question count distribution in SimuScene.

Figure 5. Distributions of topics, scenario description token counts, and VLM verification questions in the SimuScene dataset.

## B. More Related Work

**Vision–Language Benchmarks.** Complementary work has examined physics through perceptual grounding. SeePhys (Xiang et al., 2025) benchmarks diagram-centric, vision-essential QA, while PhysBench (Chow et al., 2025) evaluates multimodal understanding from videos, images, and text. Outside AI, interactive platforms such as myPhysicsLab<sup>3</sup> illustrate the feasibility of simulation-driven reasoning but are not designed around LLMs and lack textual task descriptions. These vision-language benchmarks primarily evaluate models’ ability to *interpret* existing visual content. In contrast, our work focuses on the inverse problem: *generating* visual simulations from textual descriptions via executable code. This generative capability—translating scene understanding into programmatic simulation—represents a complementary and underexplored

<sup>3</sup><https://www.myphysicslab.com/>

dimension of multimodal reasoning, requiring both comprehension and synthesis abilities.

## C. VLM Evaluation Error Analysis

To better understand the limitations of VLM-based evaluation, we analyzed the 252 disagreement cases between Qwen2.5-VL-72B-Instruct and human annotations. We identified five main error categories: *Object correspondence problems* (36%): The VLM incorrectly matches objects in the video to those described in the text. *Motion judgment inconsistencies* (35%): The VLM’s assessment of motion characteristics conflicts with actual observations. *Out-of-frame motion* (19%): Critical motion occurs outside the visible frame, while VLM returns the motion is inside the frame. *Object contact/suspension issues* (6%): The VLM fails to correctly identify whether objects are in contact or improperly suspended. *Incorrect motion direction* (4%): The VLM misjudges the direction of object movement. Representative examples are shown in Fig. 9.

## D. Implementation Details

### D.1. GRPO Optimization

We adopt Group Relative Policy Optimization (GRPO) (Shao et al., 2024). For each prompt  $x$ , the old policy  $\pi_{\theta_{\text{old}}}$  samples a group of  $K$  candidates  $c_{1:K} \sim \pi_{\theta_{\text{old}}}(\cdot | x)$  (e.g.,  $K = 8$ ). Executing each  $c_k$  produces a reward  $r_k = r(c_k | x)$  from Eq. (1). We compute a group-relative, length-invariant advantage

$$\bar{A}_k = \frac{r_k - \mu_x}{\sigma_x + \epsilon}, \quad \mu_x = \frac{1}{K} \sum_{j=1}^K r_j, \quad \sigma_x = \sqrt{\frac{1}{K} \sum_{j=1}^K (r_j - \mu_x)^2}, \quad (3)$$

and assign  $\bar{A}_k$  uniformly to all tokens of  $c_k$  to avoid length bias.

We then optimize a clipped likelihood-ratio objective *without* an explicit KL penalty, using asymmetric clipping to stabilize updates while preserving headroom for improvement:

$$\mathcal{L}_{\text{clip}}(\theta) = \frac{1}{K} \sum_{k=1}^K \frac{1}{|c_k|} \sum_{t=1}^{|c_k|} \min(\rho_{k,t}(\theta) \bar{A}_k, \text{clip}(\rho_{k,t}(\theta), 1 - \varepsilon_{\text{low}}, 1 + \varepsilon_{\text{high}}) \bar{A}_k), \quad (4)$$

where

$$\rho_{k,t}(\theta) = \frac{\pi_{\theta}(c_{k,t} | x, c_{k,<t})}{\pi_{\theta_{\text{old}}}(c_{k,t} | x, c_{k,<t})}, \quad \text{clip}(u, a, b) = \min(\max(u, a), b). \quad (5)$$

We maximize  $\mathcal{L}_{\text{clip}}$  with Adam;  $\varepsilon_{\text{low}} < \varepsilon_{\text{high}}$  (asymmetric clipping) curbs overly aggressive down-weighting while allowing moderate up-weighting of promising tokens.

### D.2. Training Data Details

The SimuScene dataset contains a total of 7,659 validated dynamic scenarios, of which 334 are reserved as a test set. For training, we use the remaining 7,325 examples. These are split into two parts:

- **Supervised Fine-Tuning (SFT):** 3,000 examples are used to fine-tune the base model with paired scenario descriptions, reasoning traces, and executable code.
- **Reinforcement Learning (RL):** the remaining 4,325 examples are used for reinforcement learning with verifiable rewards (RLVR), where VLM judgments provide reward signals.

This division ensures that the model benefits from both explicit supervised guidance and scalable reward-driven optimization.

### D.3. Dataset

We use a corpus of **7,659** samples covering five core physics domains with **52** fine-grained concept (see Table. 6). Mechanics contributes the largest share (3,533; 46.1%), followed by Electromagnetism (1,997; 26.0%), Optics (840; 11.0%), Fluid

Mechanics (724; 9.5%), and Thermodynamics (565; 7.4%). Across concepts, the mean count is 147.3 samples (median 149.5; s.d. 82.6), indicating a moderately imbalanced, long-tailed distribution.

At the concept level, *Fluid Dynamics* is the largest category (519; 6.8%), with other frequent topics including *Angular Momentum* (259; 3.4%), *gravity* (252; 3.3%), and *Electric Potential* (240; 3.1%). On the sparse end, *Inductance* (8; 0.1%), *Polarization* (10; 0.1%), *Torque* (13; 0.2%), *Coulomb's Law* (16; 0.2%), and *Simple Pendulum* (16; 0.2%) have very few examples (five concepts have < 20 samples). The ten most common concepts together account for 33.7% of the data, whereas the ten rarest account for 5.9%.

Table 6. Distribution of samples across domains and concepts

Domain	Concept	Number	Concept	Number
Electromagnetism	Electric Potential	240	Magnetic Field	200
	Electric Field	178	Capacitance	170
	Gauss's Law	169	Ohm's Law	155
	Resistance	149	Mutual Inductance	128
	Faraday's Law	127	Ampère's Law	124
	Magnetic Flux	94	Electric Current	90
	Lenz's Law	79	Self-Inductance	70
	Coulomb's Law	16	Inductance	8
			<b>Total</b>	<b>1997</b>
Fluid Mechanics	Fluid Dynamics	519	Fluid Statics	205
		<b>Total</b>		<b>724</b>
Mechanics	Angular Momentum	259	Gravity	252
	Moment of Inertia	234	Conservation of Momentum	213
	Potential Energy	208	Linear Momentum	194
	Elastic Collision	181	Linear Motion	180
	Kinetic Energy	178	Friction	172
	Damped Oscillation	159	Rotational Motion	155
	Spring Oscillator	150	Driven Oscillation	126
	Relative Motion	125	Conservation of Mechanical Energy	115
	Circular Motion	110	Curvilinear Motion	107
	Impulse	104	Inelastic Collision	102
	Elastic Force	92	Resonance	88
	Simple Pendulum	16	Torque	13
			<b>Total</b>	<b>3533</b>
Optics	Refraction of Light	226	Lens	210
	Reflection of Light	153	Interference of Light	143
	Diffraction of Light	98	Polarization	10
		<b>Total</b>		<b>840</b>
Thermodynamics	Temperature	201	Ideal Gas Law	184
	Pressure	107	Heat	73
		<b>Total</b>		<b>565</b>
		<b>Grand total</b>		<b>7659</b>

As shown in Table 6, the SimuScene dataset spans 52 concepts, which are grouped into five major domains: Mechanics (3,533 samples), Electromagnetism (1,997), Optics (840), Fluid Mechanics (724), and Thermodynamics (565), resulting in a total of 7,659 scenarios. Mechanics and Electromagnetism dominate the distribution, reflecting their central role in classical physics and their higher executability and validation success rates during data generation.

We intentionally include both well-represented concepts (e.g., Angular Momentum, Electric Potential, Refraction of Light) and low-frequency ones (e.g., Inductance, Polarization, Torque) to ensure topic diversity. This long-tail coverage allows the benchmark to evaluate LLMs not only on common physical processes but also on challenging or visually subtle phenomena, providing a more comprehensive assessment of physical reasoning.

## E. VLM as Judge vs. LLM as Judge

In this section, we compare the performance of VLM as Judge and LLM as Judge to highlight the importance of our design. For the LLM as Judge setting, we send the code produced by DeepSeek-R1-0528 directly to the Qwen/Qwen2.5-72B-Instruct(TEAM, 2024) model and augment the evaluation with two additional questions: (1) whether the code can execute

successfully, and (2) whether the code can generate and save a video. If either question receives a “False” response, the overall judgment for that item is marked as “False.”

### E.1. Agreement with human annotation

Both VLM as Judge and LLM as Judge use the same model responses. The only difference is that VLM as Judge executes the code, generates the corresponding video, and then passes the resulting video to Qwen/Qwen2.5-VL-72B-Instruct (Team, 2025), whereas LLM as Judge sends the code directly to Qwen/Qwen2.5-72B-Instruct (Team, 2024) without executing it. All other settings remain identical.

**Table. 7** reports the results on the test set compared with human annotations. True/False means the model predicted “True” while the human annotated “False,” and False/True means the model predicted “False” while the human annotated “True.” Agreement reflects the consistency between model predictions and human annotations. As shown, VLM as Judge achieves a markedly higher agreement with human annotations (87.8%) than LLM as Judge (69.1%), demonstrating the benefit of incorporating video execution and rendering into the evaluation process.

*Table 7.* Evaluation Results under Different Judges. The table shows the comparison between model predictions and human annotations. For example, *True/False* means the model predicted True while the human annotated False, and *False/True* means the model predicted False while the human annotated True. *Agreement* indicates the consistency between model predictions and human annotations.

	True/True	False/False	True/False	False/True	Agreement
VLM as Judge	613	1263	108	152	87.8%
LLM as Judge	266	1209	162	499	69.1%

### E.2. Reward design for RL training

We instantiate two reward functions to close the loop from code to video to judgment: *VLM-as-judge* variants and *LLM-as-judge* (text-only) variant. If compilation or execution fails, we set all resolved labels to 0 (negative).

**(1) VLM-as-judge: Binary (Pass/Fail) reward.** Using the same  $\mathcal{Q}_x$  and resolution rule, we define a stricter binary criterion in which a sample is marked as *pass* only if all resolved answers are positive:

$$r_{\text{binary}}^{\text{VLM}}(c \mid x) = \mathbf{1}[\forall i \in \{1, \dots, M\}, \tilde{y}_i = 1]. \quad (6)$$

This variant provides a sparse, high-precision supervision signal that is useful for ablations and thresholded evaluation.

**(2) LLM-as-judge (text-only): Pass/Fail reward.** Here we do *not* execute  $c$  nor render a video. Instead, we prompt a text-only LLM with (i) the motion description  $x$ , (ii) the generated code  $c$ , and (iii) an extended question set

$$\mathcal{Q}'_x = \mathcal{Q}_x \cup \{q_{\text{exec}}, q_{\text{video}}\},$$

where the two additional binary checks are:

- $q_{\text{exec}}$ : “Does the code execute without errors?”
- $q_{\text{video}}$ : “Does the code generate and save a video?”

The LLM is instructed to answer each question strictly with TRUE/FALSE (we parse case-insensitively and map *Yes/No* to TRUE/FALSE). Let  $z_j \in \{\text{TRUE}, \text{FALSE}\}$  denote the LLM’s answer to the  $j$ -th question in  $\mathcal{Q}'_x$ . The reward is

$$r_{\text{binary}}^{\text{LLM}}(c \mid x) = \mathbf{1}[\forall j, z_j = \text{TRUE}]. \quad (7)$$

Unlike the VLM-based variants, this setting relies solely on textual inspection of  $c$  and may disagree with actual runtime behavior; see **Table. 7** for an empirical comparison, and **Table. 8** for a quantitative evaluation.

Table 8. Performance on SimuScene under different judges.

Model	Avg@8				Pass@8			
	E.R.	R.R.	P.R.	Acc.	E.R.	R.R.	P.R.	Acc.
VLM as Judge	99.1	98.1	81.5	11.1	100.0	100.0	95.2	34.4
LLM as Judge	98.6	94.9	45.4	7.7	100.0	100.0	80.2	29.3

## F. Response Length

**Response Length for Tested Models** We further analyze the response lengths of different models on the SimuScene test set, as shown in Fig. 6. The distribution reveals a clear divide between models with and without explicit reasoning traces. Models tested with reasoning/thinking modes—including o3, DeepSeek-R1-0528, Gemini-2.5-pro, gpt-5-medium, o4-mini-high, Qwen3-32B, and Qwen3-235B-A22B—generate substantially longer responses (median  $\sim$ 2k-15k tokens), with Qwen3-235B-A22B producing the longest outputs (extending up to  $\sim$ 17k tokens), followed by reasoning-specialized models like o3 and DeepSeek-R1-0528 (median  $\sim$ 12k-15k tokens). In contrast, models tested without thinking modes—DeepSeek-V3.1, gpt-oss-20b, and gpt-oss-120b—produce much more compact responses (median  $\sim$ 1k-1.5k tokens), as they directly generate code without explicit reasoning traces. Interestingly, this substantial token overhead ( $\sim$ 10x difference) does not always translate to proportional performance gains. As shown in Table. 2, DeepSeek-R1-0528 achieves the highest Avg@8 accuracy (21.5%) with extensive reasoning traces, while GPT-5-medium reaches competitive accuracy (20.5%) with moderate token usage. More notably, compact models without thinking modes can still achieve reasonable performance: DeepSeek-V3.1 attains 14.5% accuracy and gpt-oss-120b reaches 14.0%, despite using only  $\sim$ 1/10 of the tokens. This suggests that while chain-of-thought reasoning provides benefits for complex physical simulation tasks, efficient direct code generation remains a viable approach for resource-constrained scenarios.

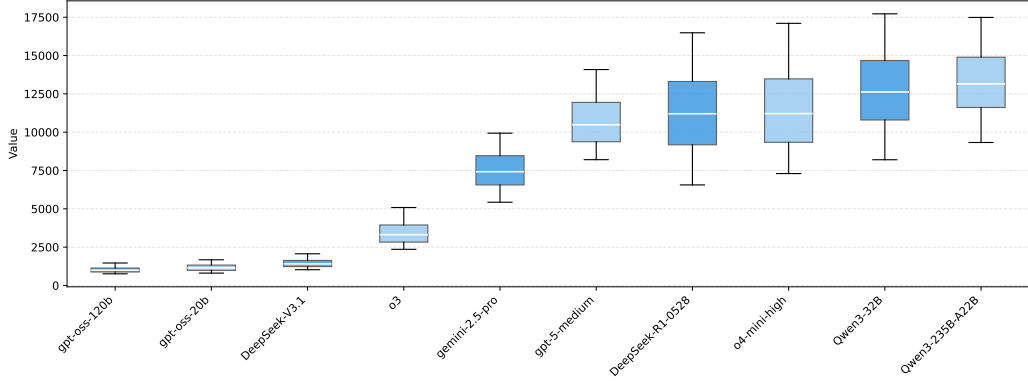


Figure 6. Distribution of response token lengths across models on the SimuScene test set. The x-axis lists models, and the y-axis reports the average token counts of their generated answers.

Interestingly, longer responses do not necessarily correlate with higher accuracy on SimuScene. For example, Gemini-2.5-pro produces the longest outputs yet achieves only moderate end-to-end accuracy (Acc. 11.5 in Avg@8), while DeepSeek-R1-0528 generates relatively shorter responses but attains the best overall performance (Acc. 20.6 in Avg@8). This suggests that verbosity alone is insufficient for physical reasoning, and that high-quality, executable code aligned with physical laws is a stronger determinant of success.

**Response Length for Trained Models** Fig. 11 shows the response length change of during RL training with different reward functions. As shown, all the lengths of three models are first decreasing, and then keeps fluctuating as the training goes on. Model initially starts at the length around 12,000, while finally keeps relatively stable between 6,000 and 9,000.

## G. More Examples

Fig. 7 presents additional representative text-to-code-to-video examples, where LLM-generated programs are executed to simulate the physical processes described in natural language. These examples highlight the diversity of dynamic scenarios

covered by SimuScene and demonstrate the feasibility of reproducing complex motions through executable code.

[Fig. 8](#) shows representative failure cases identified by the VLM-based judge. In these examples, the VLM consistently detects inconsistencies between the textual descriptions and the rendered videos, including missing or incomplete motions, object penetration through solid boundaries, and discrepancies between described and simulated dynamics. These cases demonstrate the reliability of the VLM-based judge in capturing common error modes in text-to-code-to-video pipelines, highlighting the importance of visual grounding for evaluation.

[Fig. 9](#) presents a representative disagreement case between Qwen2.5-VL-72B-Instruct and human judgments. Despite such disagreements, the overall agreement between the VLM-based judge and human evaluation reaches 87.8%, indicating strong consistency in most cases. This analysis helps identify the remaining limitations of current VLM models, particularly in handling nuanced physical or semantic inconsistencies, and provides insights for future improvements.

Finally, [Fig. 10](#) provides a side-by-side comparison of model outputs before and after RL training on the same scenario. The example demonstrates how RL training enhances the model’s ability and adherence to textual constraints, resulting in more accurate simulations. This qualitative improvement aligns with the quantitative gains observed in our benchmark evaluations.

## H. Limitations and Future Work

SimuScene currently relies on synthetic simulations and VLM-based evaluation, which may introduce model bias and does not yet cover the full richness of real-world physics (e.g. 3D lighting). Future work includes (1) expanding domains and realism (3D scenes, richer materials/forces, real videos with sensor data), (2) strengthening rewards via multi-VLM or human-in-the-loop adjudication, uncertainty calibration, and differentiable/analytic physics engines, and (3) releasing an open leaderboard and inference-time training baselines to foster reproducible progress. We hope SimuScene and RLVR provide a foundation for bridging language models and simulation scene understanding.

## I. Use of LLMs in This Work

In this work, we employ large language models (LLMs) in two primary ways. First, LLMs are integrated into the data construction pipeline, enabling the automatic generation of scenarios and verification questions. Second, LLMs are used as writing assistants to help refine and polish the manuscript.

## J. Reproducibility statement

To ensure the reproducibility of our work, we provide a detailed description of the **dataset construction pipeline** in [§ 3](#), covering scenario generation, code synthesis, and VLM-based verification. The complete **training and evaluation setup**, including model configurations, hyperparameters, and evaluation metrics, is reported in [§ 5](#), with additional ablation studies presented in the Appendix. All prompts used in our project are detailed in [§ K](#). Moreover, we include our code and scripts in the supplementary materials to facilitate replication. Together, these resources are intended to enable the community to reproduce our results and build upon SimuScene for future research.

## K. Prompt used in this paper

**Prompt Generation for Training Data** To ensure diversity and generalization for our training data, and make it to be suitable to combine with other datasets, we generate a set of prompt templates to and combine physical scenario descriptions to form the final training instructions. First, we use GPT-5 to give us a set of personalities that may need to do code simulation for physical scenarios. After manual filtering, we sample the following elements: personality, description location, and additional constraints like the code must use python and numpy. We ask GPT-5 to combine these elements to

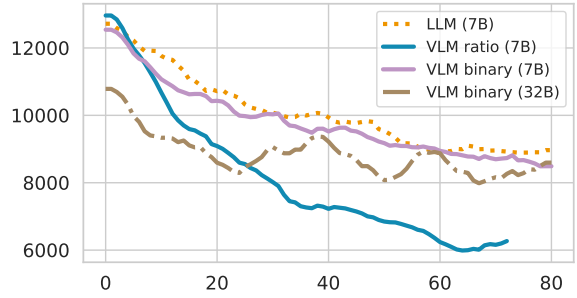


*Figure 11.* Model response length change during RL training with steps.

form the final prompt template.

**System Prompt for Code Generation**

You are an expert computational physicist specializing in scientific visualization and simulation.

You also an excellent programmer.

Your expertise includes creating educational physics simulations that effectively communicate complex physical phenomena to diverse audiences.

**User Prompt for Code Generation**

Your task is to write a Python script that generates an educational video simulating a physical process. The video will be used in academic settings to help students better understand and visualize physics concepts.

Given a textual description of a physical process:

"{content}"

Write a Python script that simulates this process and outputs a video saved as:

"name.mp4", here, "name" is a user-defined parameter passed when running the script.

Requirements for the video output:

1. Use clear and distinct colors to represent different objects, trajectories, or forces.
2. Overlay a real-time timestamp that updates continuously throughout the simulation.
3. Display all relevant parameter values (e.g., gravity, speed, angle) clearly on the screen.
4. Ensure the camera view is wide enough to fully capture the entire motion, adjusting dynamically if needed. Ensure the camera view is the best view for the simulation to let the viewer see the whole process.
5. Provide smooth and continuous animation at a consistent frame rate (30 FPS).
6. Maintain a clean, uncluttered visual style with minimal distractions and a neutral background.
7. Keep the video duration between 10 and 20 seconds, slow enough to allow viewers to observe and understand the key transitions.
8. Save the output as an MP4 video in a suitable resolution (at least 360p).
9. When the process is finish, the video should finish also.
10. Use OpenCV to generate the video, and ensure the code is correct, complete, and runnable without any errors.

Focus on clarity, interpretability, and visual appeal to make the video intuitive and easy to understand for both technical and non-technical audiences.

Physics Simulation:

- Implement precise physical equations
- Use appropriate time steps for smooth motion
- Include relevant force vectors and trajectories

The final code should:

1. Initialize all necessary libraries and variables
2. Set up the video writer with specified parameters
3. Implement the physics calculations
4. Create and save the animation
5. Include error handling and resource cleanup

Ensure the code follows PEP 8 style guidelines and includes comments explaining key components. The simulation should prioritize educational value while maintaining scientific accuracy.

Instructions:

1. Output only the complete Python code. Do not include explanations or comments. The format should be like this:

```
““python
import cv2
import numpy as np
““
```

2. The code should install the dependencies in the code.
3. The code should be runnable without any errors.
4. The code should be complete and self-contained.
5. The code should be correct and accurate.
5. The code should be efficient and optimized.
6. The code should be easy to understand and modify.

#### VLM\_as\_Judge Prompt

You are given a video and several visual verification questions. Your task is to judge each question as true or false based only on what can be seen or reasonably inferred from the video. If the visual evidence is insufficient to confirm the statement, or if the statement directly contradicts the video, answer 'false'.

#### Visual Reasoning Guidelines:

1. Perspective Changes: Objects can look different from different angles, such as a circular path may look curved, straight, or wavy depending on the viewpoint, or a cylinder may look like a circle (top view) or a rectangle (side view).
2. Simplified / Symbolic Drawings: The video may use simple shapes or colors to represent real objects. If the motion or layout still matches the description, treat it as True.
3. Container Boundaries: If no container is drawn, assume the video frame is the boundary. If a container is shown, treat it as see-through if you can see inside it. If something is not visible, don't assume it is inside the container.
4. Focus on Shape and Motion, ignore assumptions about material, weight, texture, or color. If the described motion does not match (e.g., "slides down" vs. actually moving up), answer False.
5. Occlusion: If something is partly hidden, use nearby cues to infer how it is moving or positioned.

#### Input:

- Questions: all\_questions

#### Output Format:

Return a JSON list of objects. \*\*Do not include any conversational filler or Markdown formatting tags.\*\* Fields for each object:

- "index": The question index.
- "question": The full question text.
- "analysis": A concise step-by-step breakdown of what was observed vs. what the question claims.
- "result": "true" if visually confirmed, "false" if contradicted or evidence is insufficient.

Example Format: [ "index": "1", "question": "The ball rolls along the circular path.", "analysis": "The red sphere moves in a consistent arc that completes a 360-degree loop.", "result": "true", ... ]

#### An Example Prompt Template for Training Data

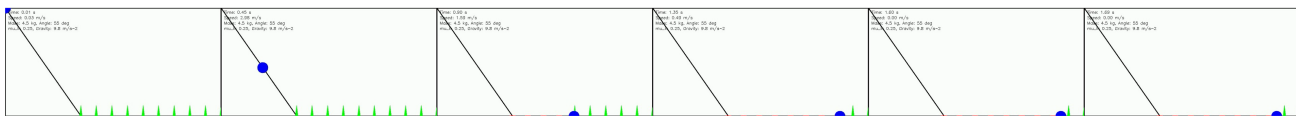
I am preparing a physics demo and need a Python script that models motion based on a textual description. Here is the scenario:

```
"{content}"
```

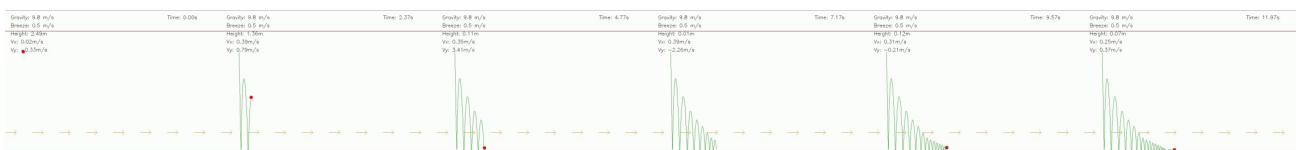
Please simulate this phenomenon in Python, render the frames with the OpenCV library, and save the resulting MP4 video to the path provided as sys.argv[1]. The code should be robust and directly runnable: include an if \_\_name\_\_

`== '__main__'` entry point, avoid interactive prompts, validate/handle missing parameters from the description, and use numerically stable time-stepping so it runs reliably end-to-end.

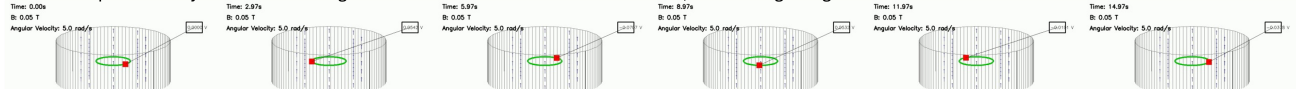
**Mechanics:** A 4.5 kg lead block is placed on a 55-degree inclined plane inside a 2-meter-long and 1-meter-high glass chamber. The plane is made of steel with a layer of fine dust, giving a coefficient of kinetic friction of 0.25. The chamber maintains a pressure of 1 atm and a temperature of 21°C with dry air. As the block slides down, it impacts a set of small, colored plastic cones arranged at the base, knocking them over sequentially.



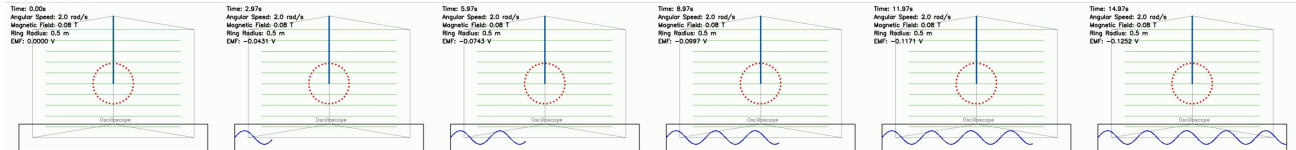
**Mechanics :** Inside a 3-meter tall glass box, a 0.15 kg steel ball is dropped from a height of 2.5 meters. The floor of the box is made of polished wood, and the ball bounces up to 1.8 meters after impact. In the box, a fan creates a gentle horizontal breeze with a constant speed of 0.5 m/s, slightly influencing the ball's rebound trajectory. This ongoing motion lasts for over 10 seconds as the ball gradually comes to a stop.



**Electromagnetism :** Inside a cylindrical glass container with a radius of 1 meter and a height of 2 meters, a solid metal ring with a radius of 0.3 meters and a mass of 2 kilograms rotates horizontally around its central axis. The inside of the container is lined with a smooth, non-conductive ceramic material. The container is filled with a uniform magnetic field of 0.05 Tesla directed vertically upwards. As the ring rotates with a constant angular velocity of 5 radians per second, it generates an electromotive force (emf) due to its motion through the magnetic field. The generated emf is measured by connecting leads to a small voltmeter attached to the ring, which is represented by a red box. The magnetic field is visualized as vertical blue lines, and the ring as a green circle.



**Electromagnetism :** In a wooden box with dimensions 2 meters by 2 meters by 2 meters, a metal ring with a radius of 0.5 meters and a mass of 3 kilograms is suspended in the center by a lightweight, insulating rod. The ring rotates around a vertical axis passing through its center at an angular speed of 2 radians per second. The box contains a magnetic field of 0.08 Tesla oriented horizontally from front to back. As the ring spins, it generates an emf due to its movement through the magnetic field, which is monitored by an oscilloscope connected to the ring. The magnetic field is represented by horizontal green lines, and the ring is depicted as a red circle.



**Optics :** Within a 1-meter-long glass tube filled with glycerin (refractive index 1.47), a triangular glass prism with a refractive index of 1.52 is placed on a flat base. The tube is sealed and laid horizontally on a lab bench. A red laser beam (650 nm) passes through an entry hole at one end of the tube, hitting the prism at an angle of 60 degrees. The light disperses into its component colors, creating a rainbow pattern along the tube's bottom. The pattern remains stable and colorful for 12 seconds, allowing for a detailed observation of the dispersion effects.



**Fluid Mechanics:** A 1 kg aluminum sphere is dropped from the top of a 2.5-meter-tall vertical glass tube. The bottom half of the tube contains a dense sugar solution, providing a visible interface and a significant increase in drag as the sphere enters. The transition from air to liquid slows the sphere noticeably, taking 16 seconds to reach the bottom while creating a vortex pattern in the sugar solution.



**Fluid Mechanics:** Within a large, transparent cylindrical aquarium with a diameter of 1.8 meters, a smooth plastic cylinder rotates horizontally at 22 rotations per minute. The aquarium is filled with saline water, with a density of 1.05 g/cm<sup>3</sup>. A small, floating green foam rectangle, with a mass of 0.15 kg and dimensions of 15 cm x 10 cm x 2 cm, is initially placed 80 cm from the cylinder. The rotating cylinder generates a circular current, drawing the foam inward. After 18 seconds, the foam reaches a stable path, orbiting the cylinder at a distance of 30 cm.

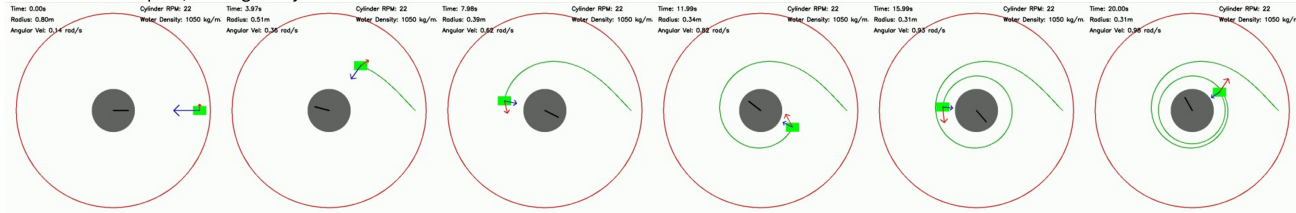


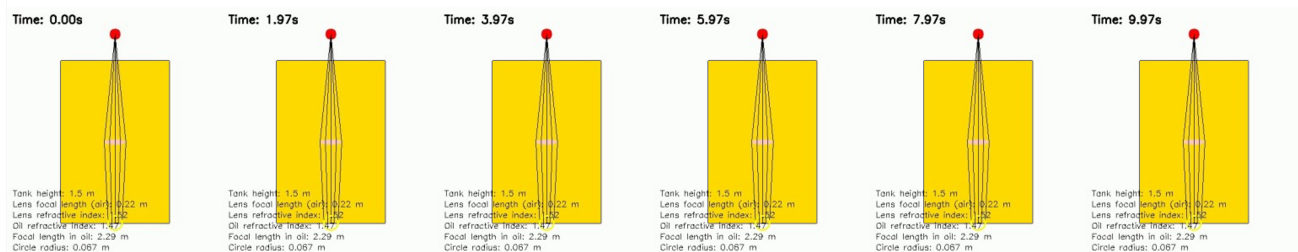
Figure 7. More representative text-to-code-to-video examples from the SimuScene benchmark. Each video is rendered from LLM-generated code to reproduce the described dynamic physical process.

**Mechanics:** In a controlled environment, a small, yellow, 0.18 kg ball is launched horizontally from a 1.2-meter-high wooden ramp inside a steel-framed enclosure with dimensions 2 m x 1 m x 1.5m. The ramp's surface has a rough texture, providing friction that limits the ball's speed to 3 m/s. The air is dry, with 20% humidity. After leaving the ramp, the ball travels for 1.6 seconds before landing on a bed of rubber pellets that absorb the impact and cause the ball to bounce slightly before settling. **Failure Question:** The entire motion of the ball occurs inside an enclosure.



**Electromagnetism:** Inside a hemispherical dome made of clear acrylic with a diameter of 1.5 meters, a charged particle of mass 1.5 grams and charge  $+1.5 \mu\text{C}$  is placed at the dome's base. The dome houses a radial electric field of  $600 \text{ N/C}$  directed from the center outward. The surface inside the dome is lined with fine sandpaper to increase resistance. The humidity is maintained at 50%. When released, the particle moves along the dome's inner surface, spiraling upwards with a gradually decreasing speed due to resistance. **Failure Question:** The particle reaches the top of the dome after its motion.

**Optics :** A 1.5-meter-high rectangular glass tank with a refractive index of 1.5 is filled with a vegetable oil solution. A 150-gram biconvex lens with a focal length of 22 cm and a refractive index of 1.52 is submerged horizontally at the center of the tank. A yellow LED light source is positioned directly above the lens, emitting a steady beam that refracts through the lens and oil. This setup creates a luminous yellow circle that appears on the tank's bottom, maintaining its form for over 10 seconds as the light persistently interacts with the lens and oil. **Failure Question:** The yellow LED light emits a steady beam through the lens and oil.



**Fluid Mechanics:** Inside a rectangular aquarium with dimensions of 100 cm by 50 cm and filled to a height of 40 cm with a transparent gel, a small stainless steel disc with a radius of 7 cm is submerged and fixed horizontally at a depth of 20 cm. The disc is rotated at a constant speed of 22 revolutions per minute by an overhead motor. The rotation of the disc generates vortices that influence the movement of suspended fine glitter particles within the gel. Over the course of 14 seconds, the glitter particles are swept into helical paths by the vortices, gradually forming concentrated, spiral formations that trace the flow patterns within the gel, showcasing the interaction of rotational motion with a semi-solid medium. **Failure Question:** The glitter particles are swept into helical paths by the vortices.



**Thermodynamics:** A light beam passes through a double convex lens inside a 75 cm high, 50 cm diameter glass cylinder filled with carbon dioxide at 1.5 atm pressure. The lens, with a refractive index of 1.55 and a focal length of 20 cm, focuses the light onto a flat black metal disk, 10 cm in diameter, located 15 cm below the lens on a roughened glass base. As the light focuses, the CO<sub>2</sub> absorbs some energy, visibly forming small, localized thermal currents in the gas above the heated disk, persisting for over 12 seconds. **Failure Question:** A light beam passes through the double convex lens inside the cylinder.

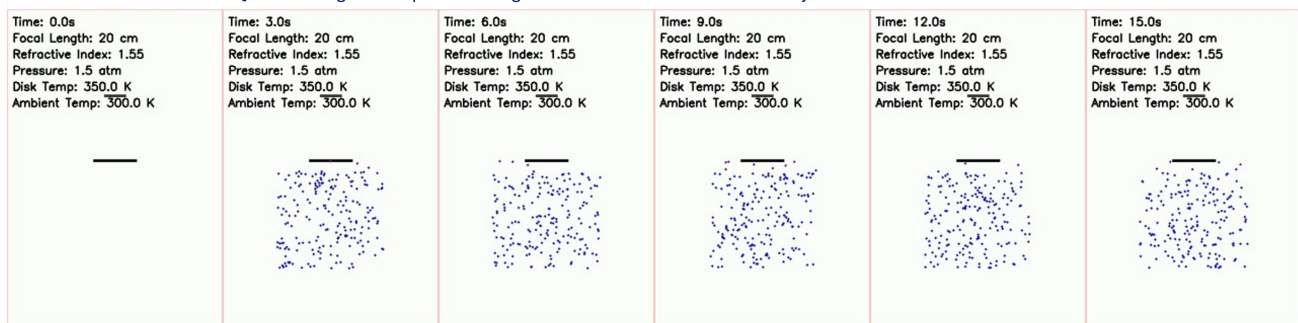


Figure 8. Representative inconsistency cases from the VLM judgement. Each example presents a text-to-code-to-video pipeline result where the VLM flagged mismatches (highlighted in blue) between the textual description and the rendered video. These failures capture common error modes, including missing or incomplete motions, object penetration through solid boundaries, and mismatches between described and simulated dynamics.

**Object correspondence problems:** Within a cylindrical chamber, a 10-gram silk ball with a charge of  $-2 \mu\text{C}$  is suspended 30 cm above a nickel capacitor plate. The chamber is filled with argon gas at 1 atm pressure and 25°C. A piston at the bottom of the chamber slowly compresses the gas over 15 seconds, increasing the pressure and thus the buoyant force on the ball. The ball rises slowly as the pressure increases.

Question: A ball is initially suspended above a plate.



--VLM: false, There is no plate visible in the video.

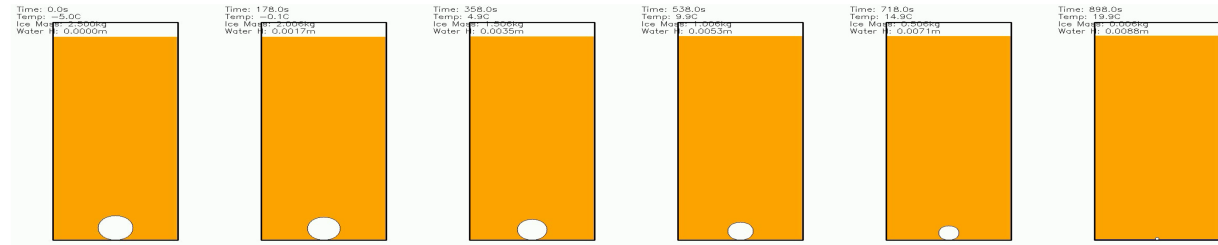
--human: true.

**Motion judgment inconsistencies:** Inside a cylindrical container, a 2.5 kg ice ball (density  $920 \text{ kg/m}^3$ ) rests on the flat base. The container is filled with pure alcohol (density  $789 \text{ kg/m}^3$ ) up to a height of 1.4 meters, so the ice ball is fully submerged and remains on the bottom. As the temperature rises, the ice ball slowly melts. The ice ball steadily decreases in size but stays in contact with the base throughout the process. The visualization shows a transparent cylindrical container, a white shrinking sphere resting at the bottom, and a light orange liquid above, with a slightly darker layer near the base representing the accumulating water.

Question: The white ball is observed to gradually melt over time.

--VLM: false, there is no indication of melting.

--human: true

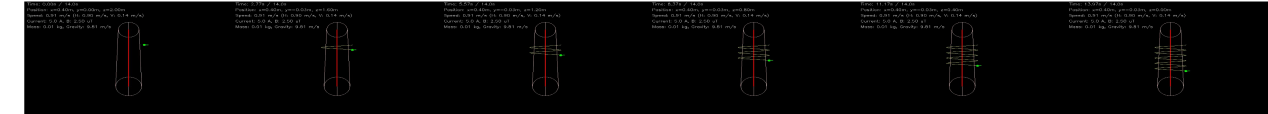


**Out-of-frame motion:** Inside a 2-meter-high glass cylinder with a diameter of 1 meter, a vertical current-carrying aluminum rod creates a magnetic field when a 5-ampere current flows through it. A lightweight, non-magnetic paper airplane with a mass of 0.01 kg is launched from the top edge of the cylinder. It glides in a circular path around the rod, descending gradually to the base over 14 seconds. The surrounding air is at standard atmospheric pressure, and the temperature is controlled at 21°C.

Question: The entire motion stays within the screen or within the drawn boundaries.

--VLM: true.

--human: false



**Object contact/suspension issues:** In a wooden box with dimensions 2 meters by 2 meters by 2 meters, a metal ring with a radius of 0.5 meters and a mass of 3 kilograms is suspended in the center by a lightweight, insulating rod. The ring rotates around a vertical axis passing through its center at an angular speed of 2 radians per second. The box contains a magnetic field of 0.08 Tesla oriented horizontally from front to back. As the ring spins, it generates an emf due to its movement through the magnetic field, which is monitored by an oscilloscope connected to the ring. The magnetic field is represented by horizontal green lines, and the ring is depicted as a red circle.

Question: After the collision, both balls oscillate together, but they are still separated by a distance.

--VLM: true

--human: false



**Incorrect motion direction:** A 0.9 kg black rubber ball rolls down a 7-degree inclined wooden board in a 3-meter-long, 1.5-meter-wide, and 1-meter-high glass enclosure. Starting at 3.5 m/s, the ball meets a 0.2 m wide area covered in dry sand, which applies a steady resistance of 0.25 N. This slows the ball steadily over 17 seconds until it stops halfway down the incline.

Question: A black ball is present at the top of an inclined.

--VLM: true

--human: false

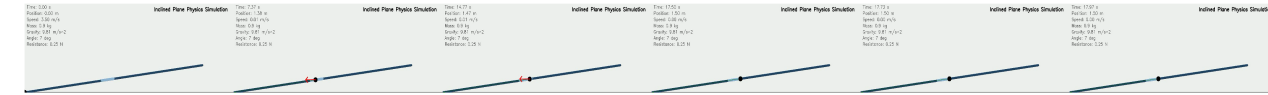


Figure 9. Representative disagreement between Qwen2.5-VL-72B-Instruct and human.

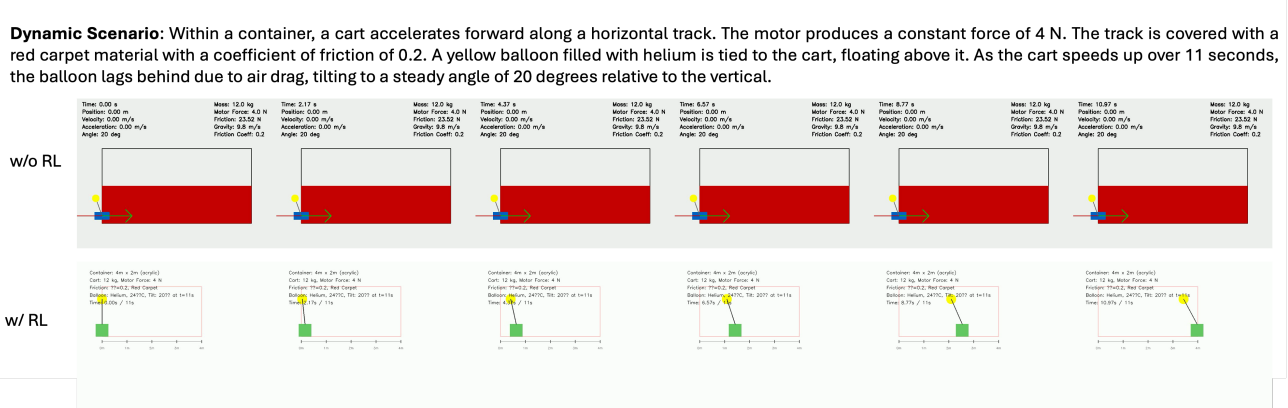


Figure 10. A text-to-code-to-video example with and without RL.